Visual Sensor-Based Measurement for Deformable Peg-in-Hole Tasks

J. Y. Kim*   and   H. S. Cho**

* Department of Robot System Engineering, Tongmyong University of Information Technology,
535, Yongdang-dong, Nam-gu, Pusan 608-711, Korea
Tel: +51-629-7236/Fax: +51-629-7249/ e-mail: kjy@tmic.tit.ac.kr
** Department of Mechanical Engineering, KAIST,
373-1, Kusong-dong, Yusong-gu, Taejon 305-701, Korea
Tel: +42-869-3213/ Fax: +42-869-3210/ e-mail: hscho@lca.kaist.ac.kr

Abstract

Unlike rigid parts, deformable parts can be deformed by contact force during assembly. For successful assembly, information about their deformation as well as possible misalignments between the holes and their respective mating parts are essential. In this paper, the locations of marks in three-dimensional space are identified by using a visual sensing system. And part deformation and misalignment in deformable cylindrical peg-in-hole tasks are measured by using the sensing system. Experimental results show that the system and the measurement algorithm are effective in measuring part deformation and misalignment, thereby dramatically increasing the success rate in assembly operations.

Key words : Deformable parts assembly, Visual sensing system, Part deformation, Misalignment, Cylindrical peg

1. Introduction

For successful assembly of deformable parts, informations about their deformation as well as possible misalignments between the holes and their respective mating parts are essential. However, because of the nonlinear and complex relationship between parts deformation and reaction forces, it is difficult to acquire all required informations from the reaction forces alone. Such informations can be acquired from visual sensors.

Compared with a variety of research in the area of rigid parts assembly [1,2], not much research has been done on deformable parts assembly [3]. In addition, none of the works measured both of part deformation and misalignment between the mating parts. Motivated by this, the authors have presented a visual sensing system that can detect three-dimensional part deformation and misalignment in previous work [4]. And the authors have presented an algorithm to measure

part deformation and misalignment by using the sensing system in cylindrical peg-in-hole tasks [5]. The proposed sensing system can obtain three-dimensional information, even though only one camera is used.

In this paper, a series of experiments to identify the locations of marks in three-dimensional space, and to measure part deformation and misalignment are performed. Through these experiments, the measurement accuracy of the system is investigated as one of its performance.

This paper is organized as follows: In section 2, the configuration and the specifications of the visual sensing system are described. In section 3, a series of experiments to identify the locations of marks in three-dimensional space using the sensing system are performed. In section 4 and 5, the algorithm to measure part deformation and misalignment using the sensing system is described. And a series of experiments to measure part deformation and misalignment in cylindrical peg-in-hole tasks are performed. The experimental results and discussions are described. Finally, some conclusions are made in section 6.

2. A Visual Sensing System

2.1. Configuration

Fig. 1(a) illustrates the basic configuration of the sensing system. It is composed of a camera, a pair of plane mirrors, and a pair of pyramidal mirrors. In order to measure three-dimensional deformation by using a camera, two views are necessary, as shown in Fig. 1(b). Fig. 1(c) illustrates an image of a peg and a hole pair. Because four images that are reflected from each face of the pyramidal mirrors are projected on the image plane of a camera, this system configuration is equivalent to that utilizes four cameras. This configuration allows the system to overcome self-occlusion.

2.2. Specifications

2.2.1. The field of view

(a) the sensor configuration   (c) a typical image and its four divisions
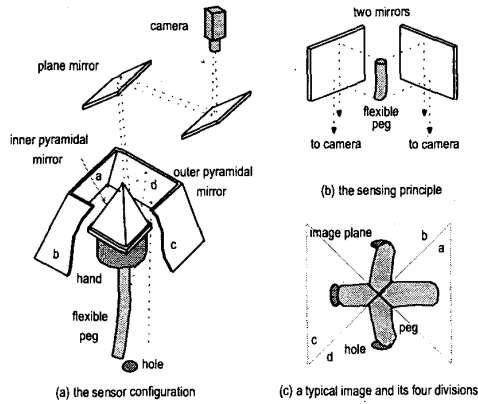
(b) the sensing principle

Fig. 1. The schematic of the sensing system

The field of view(FOV) of the system is obtained from the FOVs corresponding to each face of the pyramidal mirrors. Because the system uses stereo vision, the effective FOV V_e that can be seen through two or more faces of the pyramidal mirrors is actually available for three-dimensional measurement. Hereafter, what is referred to as the FOV means the effective FOV. The omni-directional FOV V_o is the region that can be seen through all faces of the pyramidal mirrors.

$$V_e = (V_a \cap V_b) \cup (V_a \cap V_c) \cup (V_a \cap V_d)$$
$$\cup (V_b \cap V_c) \cup (V_b \cap V_d) \cup (V_c \cap V_d) \tag{1}$$

$$V_o = V_a \cap V_b \cap V_c \cap V_d \tag{2}$$

Because most objects have height, characteristics of the system should be investigated in three-dimensional space. It is also necessary to investigate characteristics and specifications on the two-dimensional plane, for example, the hole plane. Therefore, in consideration of a representative measurement height, we defined the reference plane as the object plane that has a working distance of 508 mm. Fig. 2(a) shows the three-dimensional FOV, and Fig. 2(b) shows the two-dimensional FOV on the reference plane.

2.2.2. The depth of field and resolution

The depth of field D can be calculated by the following equation [6]:

$$D = \frac{2wacf(w-f)}{a^2 f^2 - c^2 w^2} \tag{3}$$

where w is the working distance, f is the focal length, a is the diameter of the aperture, and c is the allowable

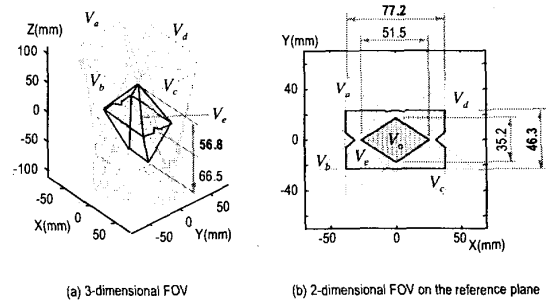(a) 3-dimensional FOV   (b) 2-dimensional FOV on the reference plane

Fig. 2. The field of view of the implemented sensing system

confusion diameter. In the implemented system, the depth of field is greater than the variation in working distance. Therefore, all points in the FOV can be focused within a pixel size on the image plane. On the other hand, resolution R is given by

$$R = \frac{V}{n_e} \tag{4}$$

where V is the size of the FOV, and n_e is the number of pixels in V. Resolution of the implemented system varies with the locations in the FOV. Therefore we define that the standard resolution R_s is the smallest resolution in the inside region of the circle with the radius of 10 mm centered at the middle of the FOV. In the implemented system, R_s is about 0.2 mm.

3. Measurement of the Locations of Marks

In this section, the measurement accuracy of the implemented system in identifying the locations in three-dimensional space is investigated. A series of experiments for measuring the locations of the circle-shaped marks at any height are performed by using a test sheet, as shown in Fig. 3. They were measured at three different height at intervals of 10 mm.

When a mark is reconstructed in the three-dimensional object space for the identification of its location, there is the possibility that the optical paths corresponding to a couple of the projection points in the image plane don't intersect at one point. This is caused by image noises, the inaccurate parameters, the limitation of sensor resolution, and so on. In such a case, the nearest point to the epipolar line from the actual projection point is approximated to the new corresponding point.

Fig. 4 shows the projected images and the reconstructed marks of the original marks on the test

sheet. Table 1 shows the measurement errors in projection to the image plane, which are the differences between the actual projected locations and the locations calculated theoretically from the calibrated system parameters. This table shows the errors according to the measurement height, and according to the division in the image plane. The average value of the errors of all the cases is about 0.027 mm, which corresponds to two pixels in the image plane.

Table 2 shows the measurement errors in identifying the locations of the marks, which are the differences between the actual locations and the locations identified by the system. This table shows the errors according to the measurement height, and according to which set of two images are selected among the four corresponding to four divisions each of the image plane. The average value of the errors of all cases is about 0.763 mm, and the average value of the three cases that a set of two divisions with the minimum error are selected is about 0.609 mm. They correspond to three or four pixels in the image plane.
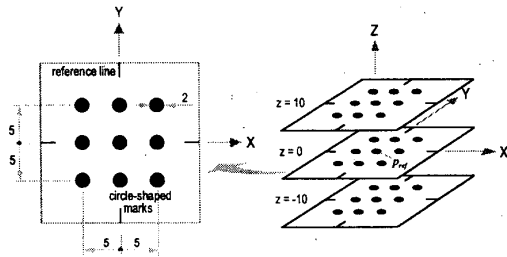
is obtained by using an image grabber. Next, the edge image is extracted from the raw image. Next, the image plane is divided into four divisions corresponding to each view. Next, pegs and holes are separately recognized in each division. Next, the coordinates of the pegs and the holes in the screen coordinate system are transformed into the coordinates in the image plane coordinate system. Finally, the peg and the hole are

Table 1. Error in projection of marks

(unit : mm)

item		view 'a'	view 'b'	view 'c'	view 'd'	average of 4 views
z = 0	average	0.020	0.020	0.036	0.024	
	min	0.005	0.007	0.024	0.003	0.025
	max	0.031	0.037	0.049	0.046	
z = 10	average	0.025	0.017	0.037	0.023	
	min	0.010	0.003	0.026	0.010	0.026
	max	0.037	0.024	0.050	0.033	
z = -10	average	0.016	0.034	0.025	0.048	
	min	0.005	0.015	0.011	0.025	0.031
	max	0.024	0.053	0.035	0.072	
average of 3 z-values	average	0.020	0.024	0.033	0.032	0.027

Table 2. Error in reconstruction of marks

(unit : mm)

item		view 'ab'	view 'ba'	view 'bc'	view 'cb'	view 'cd'	view 'dc'	view 'da'	view 'ad'	average of 8 views
z = 0	average	0.428	0.477	0.568	0.708	0.747	0.677	0.517	0.551	
	min	0.174	0.214	0.274	0.479	0.477	0.440	0.175	0.378	0.584
	max	0.646	0.786	0.895	0.929	1.090	0.956	0.965	0.787	
z = 10	average	0.665	0.62	0.869	0.934	1.021	0.936	0.471	0.498	
	min	0.427	0.440	0.740	0.774	0.651	0.808	0.182	0.195	0.752
	max	0.871	0.870	1.114	1.134	1.393	1.076	0.659	0.739	
z = -10	average	0.733	0.899	0.797	0.794	0.78	0.989	1.385	1.258	
	min	0.580	0.650	0.507	0.684	0.514	0.490	0.970	1.029	0.954
	max	0.931	1.190	1.109	0.906	1.035	1.478	1.779	1.524	
3 z-values	average	0.609	0.665	0.744	0.812	0.849	0.867	0.791	0.769	
	min	0.467	0.482	0.561	0.675	0.677	0.674	0.584	0.631	0.763
	max	0.717	0.881	1.014	0.981	1.058	1.133	1.101	0.944	

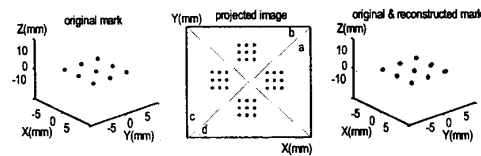Fig. 3. The test sheet for measuring the locations of marks

Fig. 4 Experimental projection and reconstruction of the marks

4. Measurement of Part Deformation

In order to investigate the measurement performance of the sensing system, a series of experiments to measure part deformation and misalignment in cylindrical peg-in-hole tasks were performed. Fig. 5 shows the measurement procedure using the proposed sensing system. First, the raw image of a peg and a hole
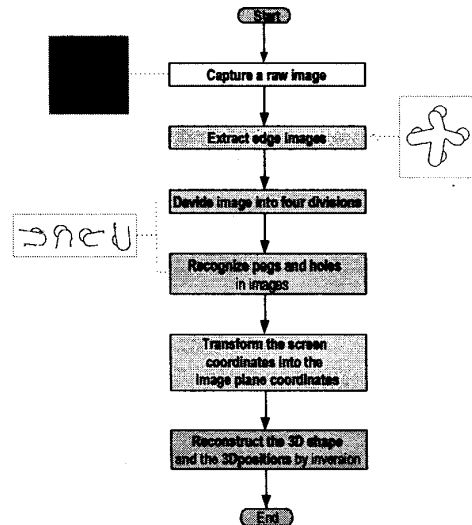

Fig. 5. The procedure for measuring part deformation and misalignment

reconstructed in the three-dimensional space by using a stereo principle.

The deformation of a cylindrical peg is estimated from the shape of the center-line of the peg. The algorithm is shown in Fig. 6, and the detailed method was described in previous work [5].

Fig. 7(a)-(c) show the projected images and the measurement errors of the inclined pegs when $\phi = 0°$, $e = 0,3,6\,mm$. In these figures, ϕ is the azimuth angle of the bottom of a peg, namely, the direction of misalignment between the hole and its respective mating peg. And e is the size of misalignment. The measurement error is varied according as which set of two divisions are selected from four divisions of the image plane. The thick lines in the figures represent the cases the measurement error at the bottom of a peg is minimum.

Fig. 7(d)-(f) show the measurement errors when $\phi = 45°, e = 0,3,6\,mm$. As shown in Fig. 7(f), some edges in the a-division and the b-division of the projected image of a peg were omitted because part of the peg exists outside the field of view. This is the reason that the measurement error in the cases the a-division or the b-division is selected is much larger than that in the others. On the other hand, there is little difference in the measurement error according as which divisions are selected unless it is the case some information is omitted like Fig. 7(c) or 7(f). Excepting such cases, the measurement error at the bottom of a peg is less than 1 mm, and the measurement error throughout the whole length of a peg is less than about 1.5 mm. These errors are primarily caused by image noises.
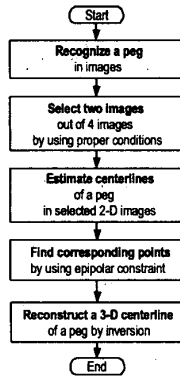

Fig. 6. Algorithm to measure the deformation of a cylindrical peg

5. Measurement of Misalignment

(—— : when the measurement error at the peg bottom is minimum
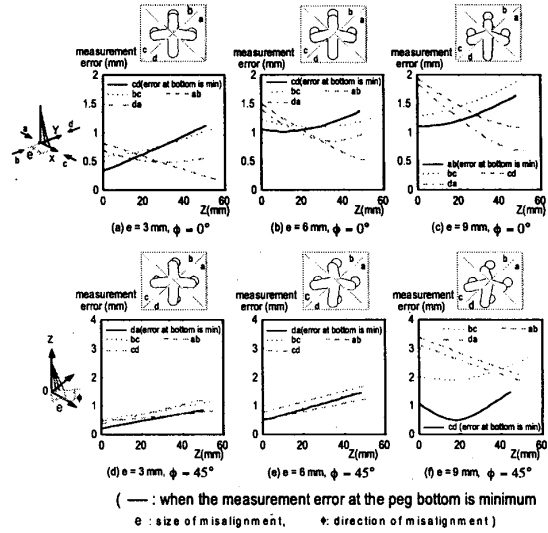e : size of misalignment,   ♦: direction of misalignment)

Fig. 7. Experimental results of measurement of part deformation according to the selection of two views

Misalignment between mating parts is defined as the relative error between the center of a hole and the center of the bottom of a peg. Fig. 8 shows the algorithm to estimate misalignment and the algorithm to estimate the center of an occluded hole.

Three-dimensional measurement by stereo vision requires two views whose directions are different each other. The proposed sensing system has views in four directions so that it can overcome occlusion. In consequence, it is necessary to select a set of two views that have the most information, namely, ones that show the most on the hole and the peg. In case of a peg, its visible part varies according to viewing direction, but each size is about the same. In case of a hole, however, the size of its visible part is very sensitive to viewing direction because occlusion by its respective mating peg is occurred. Therefore, only a hole is taken into consideration as the condition of selection of views, and a set of two views that have most in common were selected.

Fig. 9 shows the hole edges which is seen in common according to the selection of two views, namely, two divisions of the image plane. The azimuth angles ψ_s^{ab}, ψ_t^{ab} corresponding to the start and the end of the common edge of the a-division and the b-division are given by

$$\psi_s^{ab} = \max(\psi_{as}, \psi_{bs})$$
$$\psi_t^{ab} = \min(\psi_{at}, \psi_{bt}) \tag{5}$$

570

$$\psi^{ab} = \begin{cases} 0 & if \quad \psi_t^{ab} - \psi_s^{ab} < 0 \\ \psi_t^{ab} - \psi_s^{ab} & if \quad 0 \le \psi_t^{ab} - \psi_s^{ab} \le 360 \\ \psi_t^{ab} - \psi_s^{ab} - 360 & if \quad 360 < \psi_t^{ab} - \psi_s^{ab} \end{cases} \quad (6)$$

The longest edge, namely, the edge that have the most information has the greatest angle range. Therefore, a set of two divisions are selected on the basis of the angle range, which is given in Eq. (6).

Fig. 10(a) shows the errors in measuring the centers of the bottoms of the pegs when $e = 0, 3, 6, 9\ mm$ in case $\phi = 0°$, $\phi = 45°$. This figure shows the maximum errors and the minimum errors according as which set of two divisions are selected. The minimum errors are less than 1 mm. Fig. 10(b) shows the errors in measuring the inclination at the bottoms of the pegs on the same condition as Fig. 10(a). The minimum errors are less than $1.5°$.

(a) estimation of misalignment

(b) estimation of a hole center

Fig. 8. Algorithm to measure misalignment

(a) the original peg and the hole

(b) the projected image

(c) common edge image

selected views	edges in each view	common edge
a + b		ψ_s^{ab} ψ_t^{ab}
b + c		ψ_s^{bc} ψ_t^{bc}
c + d		ψ_s^{cd} ψ_t^{cd}
d + a		ψ_s^{da} ψ_t^{da}
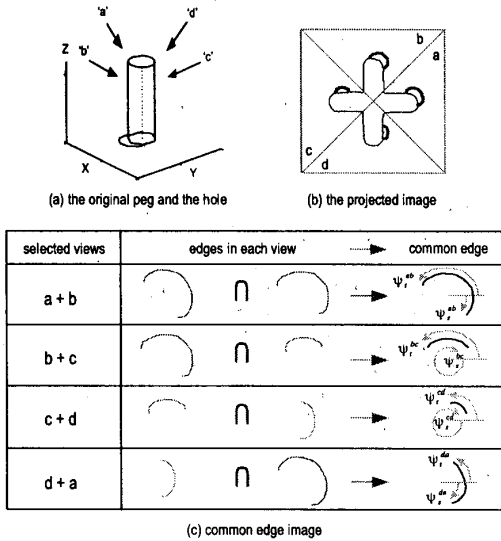
Fig. 9. Selection of two edge images from the four

measurement error (mm)

(1) $\phi = 0°$

(2) $\phi = 45°$

(a) estimation of the center of the peg bottom

measurement error (deg)

(1) $\phi = 0°$

(2) $\phi = 45°$

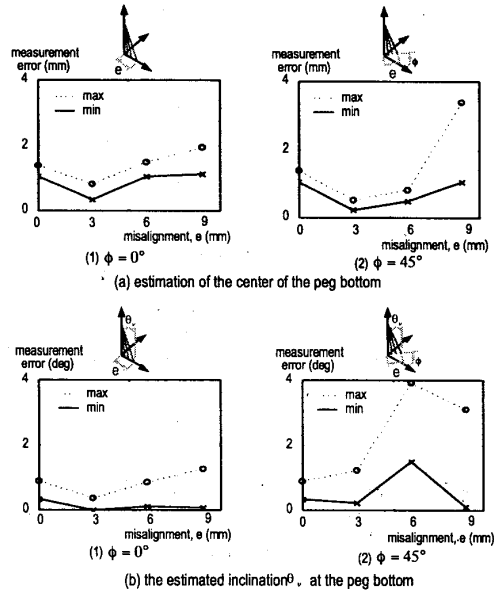(b) the estimated inclination θ, at the peg bottom

Fig. 10. Experimental measurement results about pegs

where ψ_{as}, ψ_{at}, ψ_{bs}, ψ_{bt} each is the azimuth angle corresponding to the start, the end of the edge in the a-division, the b-division. Their values are given in such a way that $\psi_{at} \ge \psi_{as}$, $\psi_{bt} \ge \psi_{bs}$. They can be set on the basis of the hole centers, which are estimated by using the approximated conic equations of the hole edges. The angle range ψ^{ab} corresponding to ψ_s^{ab} and ψ_t^{ab} is obtained by

Fig. 11(a) shows the errors in measuring the centers of the occluded holes on the same condition as Fig. 10. This figure shows the maximum errors, the minimum errors, and the errors of the case where a set of two divisions that have most in common are selected. The size of the errors is varied, depending on which divisions are selected out of the four. The minimum errors are less than 1 mm when $\phi = 0°$, less than 1.6 mm when $\phi = 45°$.

Fig. 11(b) shows the errors in measuring the lateral

misalignment between the hole and its respective mating peg. This figure also shows the maximum errors, the minimum errors, and the errors of the case where a set of two divisions that have most in common are selected. The minimum errors are less than 0.6 mm when $\phi = 0°$, less than 2.5 mm when $\phi = 45°$. The measurement error of the case $e = 9\,mm$ in Fig. 11(b2) is much larger than the other cases. This is because the partial edge of the peg is omitted, as described in section 4. The minimum errors are less than 0.7 mm excepting such a case.

From these results, it can be determined that the proposed sensing system with multi-views can be used more effectively in the cases where occlusion occurs. As described in section 4, the measurement errors in these experiments are primarily caused by the image noises, too.
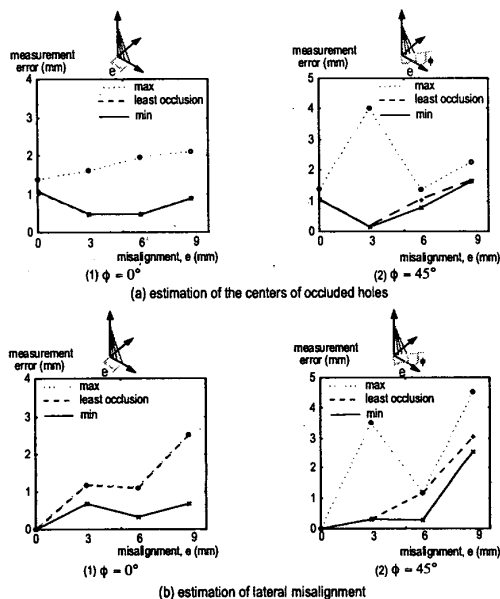
measurement errors corresponding to about three or more pixels in the image plane. These measurement errors are primarily caused by the image noises, by the limitation of the system resolution, by the inaccurate parameters, and so on. From the experimental results, it is concluded that the sensing system and the measurement algorithm are available for the measurement of part deformation and misalignment. In particular, they are more available to the assembly tasks that occlusion is occurred. In further research, flexible parts assembly by using the implemented sensing system and by using the sensor fusion will be performed.

References

[1] D. E. Whitney, "Quasi-Static Assembly of Compliantly Supported Rigid Parts", *ASME J. Dyn. Syst. Measur. Control*, vol. 104, pp. 65-77, 1982.

[2] Y. K. Park and H. S. Cho, "Fuzzy Rule-based Assembly Algorithm for Precision Parts Mating", *Mechatronics*, vol. 3. pp. 433-450, 1993.

[3] H. Nakagaki, *et. al*, "Study of Insertion Task of a Flexible Wire into a Hole by Using Visual Tracking Observed by Stereo Vision", *Int. Conf. on Robotics and Automation*, pp. 3209-3213, 1996.

[4] J. Y. Kim, H. S. Cho, and S. Kim, "A Visual Sensing System for Measuring Parts Deformation and Misalignments in Flexible Parts Assembly", *Optics and Lasers in Engineering*, Vol. 30, No. 5, pp. 379-401, 1998.

[5] J. Y. Kim, H. S. Cho, and S. Kim, "Measurement of Parts Deformation and Misalignments by Using a Visual Sensing System", *IEEE Int. Sym. on Computational Intelligence in Robotics and Automation*, pp. 362-367, 1997.

[6] E. Krotkov, "Focusing", *Int. J. of Computer Vision*, Vol. 1, pp. 223-237, 1987.

Fig. 11. Experimental measurement results about holes

6. Conclusions

In this paper, a series of experiments to identify the locations of the marks, and to measure the parts shape and misalignments in cylindrical peg-in-hole tasks were performed by using a visual sensing system [4]. This system measures part deformation in any direction and misalignment between mating parts without use of an analytical model.

The experimental results in identifying the locations of the marks and in measuring misalignments show the